NASA CR-54373
4163-6012-SU-000

MICROMETEORITE BOMBARDMENT INITIATING DISCHARGES AND BREAKDOWN IN ION THRUSTORS

by

J. C. Slattery

Prepared for

NATIONAL AERONAUTICS AND SPACE ADMINISTRATION

CONTRACT NAS 3-5755

TRW SPACE TECHNOLOGY LABORATORIES

NASA CR-54373
4163-6012-SU-000

SUMMARY REPORT

MICROMETEORITE BOMBARDMENT INITIATING DISCHARGES AND BREAKDOWN IN ION THRUSTORS

by

J. C. Slattery

prepared for

NATIONAL AERONAUTICS AND SPACE ADMINISTRATION

24 May 1965

Contract NAS 3-5755

Technical Management
NASA Lewis Research Center
Cleveland, Ohio
Spacecraft Technology Division
John Ferrante

TRW Space Technology Laboratories
One Space Park · Redondo Beach, California

MICROMETEORITE BOMBARDMENT INITIATING DISCHARGES AND BREAKDOWN IN ION THRUSTORS

by

J. C. Slattery

ABSTRACT

28875

The characteristics of arcing induced by the impact of a micron-sized hypervelocity particle in a simulated ion engine was examined. The work pertains to the threat of damage to spacecraft from micrometeorites in outer space. For several ion engine voltages, the probability of discharge formation was measured in clean systems and in the presence of cesium. Damage caused by an arc was examined photographically for tungsten, copper and aluminum electrodes and the effectiveness of a proposed electrical filter was assessed. The free charge produced by a hypervelocity impact was measured for carbon particles and the ion species tentatively identified.

Auth

TABLE OF CONTENTS

LIST OF FIGURES

LIST OF FIGURES (continued)

MICROMETEORITE BOMBARDMENT INITIATING DISCHARGES AND BREAKDOWN IN ION THRUSTORS

by J. C. Slattery

TRW Space Technology Laboratories

SUMMARY

In outer space, near the earth, the expected meteoroid flux of micron-sized particles is several per second per square meter. This high flux rate makes it important to predict any adverse effects from these micrometeorite impacts. Previous work at Space Technology Laboratories has established the fact that a microparticle impact can produce an electrical discharge in a simulated ion engine under certain conditions.

The work reported on here was undertaken to establish the probabilities of discharge formation and the arc characteristics.

The free charge produced by a hypervelocity impact was measured for tungsten and copper targets with carbon and iron bombarding particles. The charge carriers have been identified as electrons and ions of particle material (either iron or carbon). No evidence was found that ions of target material were produced.

The probability of an impact causing an arc to form was measured in a simulated ion engine for voltages up to 9 kV, both with and without the presence of cesium. The probability is zero to about 4 kV and increases to 50% at 9 kV. The presence of cesium raises the probabilities slightly at the lower voltages but appears to have little effect at the higher voltages.

Arc damage was examined photographically for electrodes of tungsten, copper and aluminum. The damage appeared to be very slight if electrical filters were used to limit the available energy.

I. INTRODUCTION

Under a previous NASA Contract (NAS3-3569), Space Technology Laboratories conducted an investigation into the mechanism of charge production by hypervelocity impact. The results of this work are contained in a NASA report, No. CR-54057. In addition to quantitative measurements on the effects of various target parameters, these experiments established the fact that, under certain conditions, microparticle impacts could initiate an electric discharge in a simulated ion thrustor.

The work under the present contract was undertaken to establish more precisely the conditions of arc formation. The damage to various electrode materials caused by the discharge was also examined, as was the effect of external circuitry on the arc damage.

The simulated micrometeoroids were obtained from the STL hypervelocity accelerator, a modified 2-Million-Volt Van de Graaff generator. The accelerated particles were usually iron spheres, about a micron in diameter, although carbon particles were used for some of the experiments. Particle velocities ranged from two or three km/sec up to about 30 km/sec. These velocities are a little lower than expected for natural meteorites, but the size of the particles is appropriate. The expected meteoroid flux of one micron particles in the vicinity of the earth is several per second per square meter. This high flux rate makes it important to predict in advance any adverse effects due to these small particle impacts.

II. EXPERIMENTAL APPARATUS

The STL hypervelocity accelerator is a 2 MV Van de Graaff generator. A contact charging process places a high charge on micron-sized iron (or carbon) grains and they are then accelerated through the Van de Graaff voltage. The particles arrive at the experiment one at a time and each one is observed with a detector.

The detectors are usually cylinders coaxial to the particle beam connected to a high impedance amplifier. The particle charge induces a voltage on the detector capacitance. The height of the voltage signal is proportional to the particle charge and the length of the signal gives the transit time through the detector. Knowing the charge, velocity and accelerating voltage, the particle mass can be calculated by equating the electrostatic potential energy, qV, to the particle kinetic energy. Since there is a spread in the size and velocity of the particles this measurement is made for each particle used in an experiment. If only a few particles are involved in an experiment, data collection is done by photographing an oscilloscope trace for later analysis. In the experiments involving large numbers of particles, such as the discharge measurements described further on in this report, data collection was by means of an electronic x-y plotter.

This device plots each particle as a point on an oscilloscope screen with the y-axis proportional to the particle charge and the x-axis proportional to the transit time of the particle through a detector (reciprocal velocity). Each particle is plotted as a point representing a unique mass and velocity. Lines of constant mass can then be drawn on the plot and the mass represented by any point can be quickly identified. It still remains to identify those particles causing a discharge.

The display of particle parameters in the absence of discharge is simple since particle detectors supply a pulse whose height is proportional to charge and whose length is the time to pass through a detector. The maximum pulse height of the pulse is clamped with a diode and fed to the vertical deflection plates of an oscilloscope and at the same time the scope sweep is triggered. When the pulse ends a brightening spike is applied to the scope cathode. The scope intensity is arranged so that only the dot which occurs when the brightening pulse is applied can be seen.

When a discharge experiment is being performed, this method is modified somewhat. The reason for this is that it is not known whether or not a particle causes a discharge until some time after it passes through the detector. If a particle does cause a discharge it is written on the oscilloscope as a short line instead of a dot. Thus, it is necessary to delay the displaying of a given particle until it is known whether or not this particle causes a discharge.

Figure 1 illustrates schematically the method used to delay the display for 100 microseconds and the means of displaying it either as a dot for no discharge or as a short line for a discharge. Referring to Fig.1, it is seen that a pulse from a particle detector is delivered first to the y-axis of an oscilloscope through a blocking diode so that the beam is deflected upwards an amount proportional to the charge of the particle. Secondly, the pulse is delivered to the time delay network. It is differentiated at the input and the positive spike which represents the leading edge of the pulse triggers a 100 microsecond univibrator. The trailing edge of this 100 microsecond pulse is used to start the oscilloscope sweep. At the same time, the trailing edge of the detector pulse is used to trigger another 100 microsecond univibrator and the trailing edge of this pulse triggers a trace brightener which in turn will brighten the oscilloscope beam. The trace brightener has two time constants and which time constant is actually used is determined by a gate, which is triggered by a signal from the discharge experiment. If no discharge occurs, then a short time constant trace brightener pulse is applied. On the other hand, if a discharge occurs the gate is opened and the trace brightener pulse is made longer. In this way information displayed is written as a dot for no discharge and as a short line when a discharge has occurred.

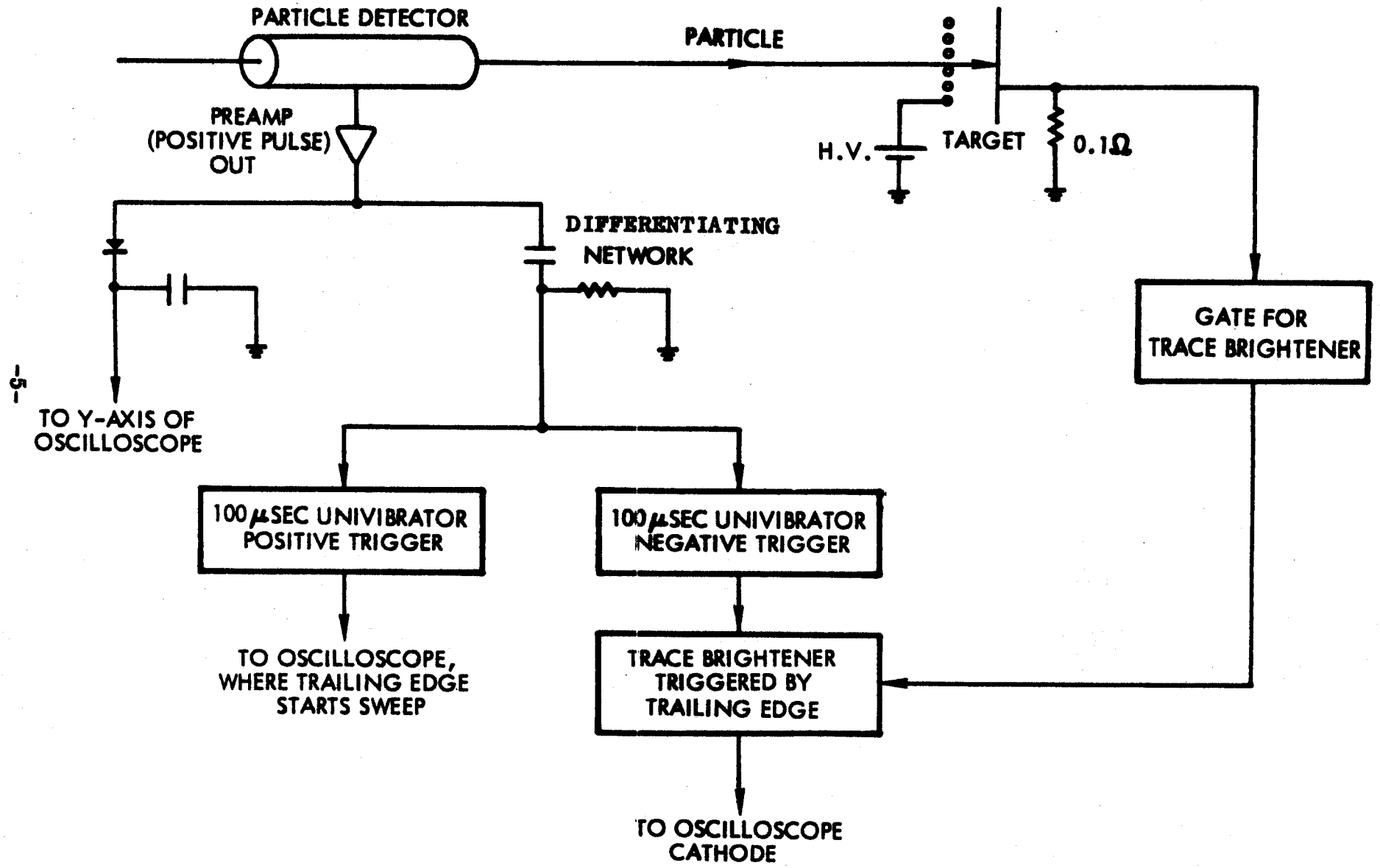

Figure 1. Schematic diagram of experiment to determine parameters of hypervelocity particles producing discharges in simulated ion engines.

III. EXPERIMENTS ON CHARGE YIELD

A. CHARGE PRODUCTION BY CARBON PARTICLES

One of the first experiments performed was a measurement of the free charge produced by the impact of carbon particles on targets of tungsten and copper. The charge yield from carbon particles was measured in a way similar to that described in NASA Report, No. CR-54057. The target to be bombarded was positioned 0.150" away from a 100-mesh, 0.001" wire tungsten grid and 300 volts was applied to the grid. Particles were injected through the grid and impacted on the target. The amount of free charge created was measured by the voltage change of the target as electrons flowed to the grid.

These data are shown in Figs. 2 (tungsten target) and 3 (copper target). The ordinate in both cases is the charge yield normalized to the impacting particle mass while the abscissa is particle velocity. For convenience a dotted line is included on each graph which is an eyesight fit to the data obtained earlier with iron particles on the same target materials. There appears to be only a slight difference between iron and carbon particles.

B. EFFECT OF SURFACE ELECTRIC FIELD

An experiment to evaluate the effect of target surface roughness was performed using three different molybdenum targets. Microscope photographs of the three targets are shown in Fig. 4 with a magnification of 400X. Figure 4a shows the "smooth" target, with a surface essentially as received from the supplier. Although there are long scratches, presumably due to the rolling operation on the metal, the protrusions above the surface are all of the order of one micron or less. Figure 4b shows a medium-rough carborundum grit. The result is a uniformly roughened surface with hills and valleys which appear to be about five microns deep. Figure 4c shows a very rough target, made by pressing with a large carborundum grit. The craters are about 50 microns in diameter, with an average spacing of about 100 microns. There are protrusions on most of the craters which are about 25 microns deep.

The experiment consisted of measuring the charge yield due to particle impacts from each of these targets under identical conditions. A 100-mesh tungsten grid was positioned 0.150" away from the target and 300 volts was applied to the grid. The average field in the gap was thus 800 volts/cm. The different surface conditions should have changed the local field at the target surface considerably.

The charge yield was detected at the target. The voltage polarity was such that ions left the target and the target

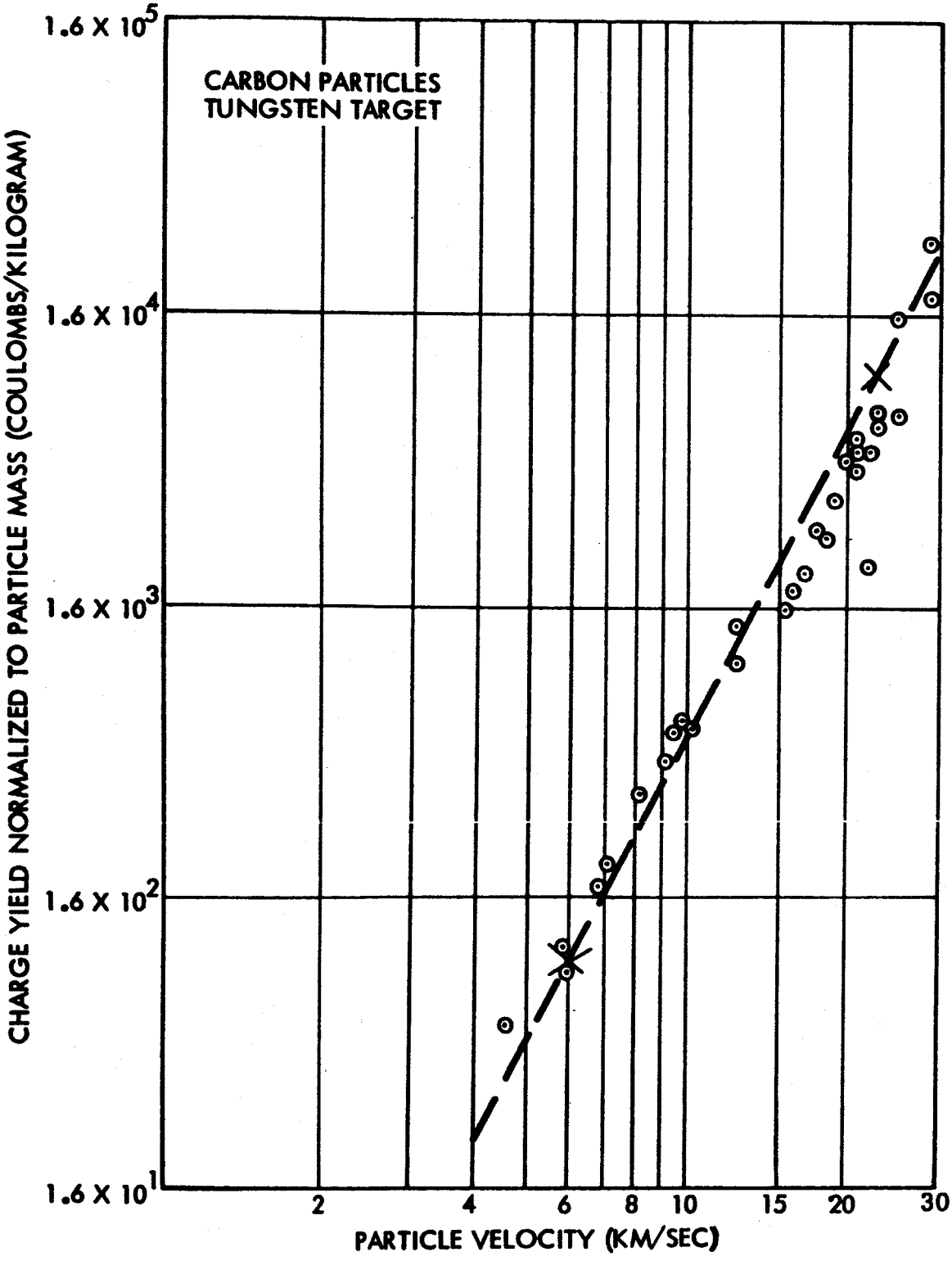

Figure 2. Charge Yield, Normalized to Particle Mass, from Carbon Particles Impacting on a Tungsten Target as a Function of Particle Velocity. Dotted line is an approximate fit to previous data using iron particles on the same target material.

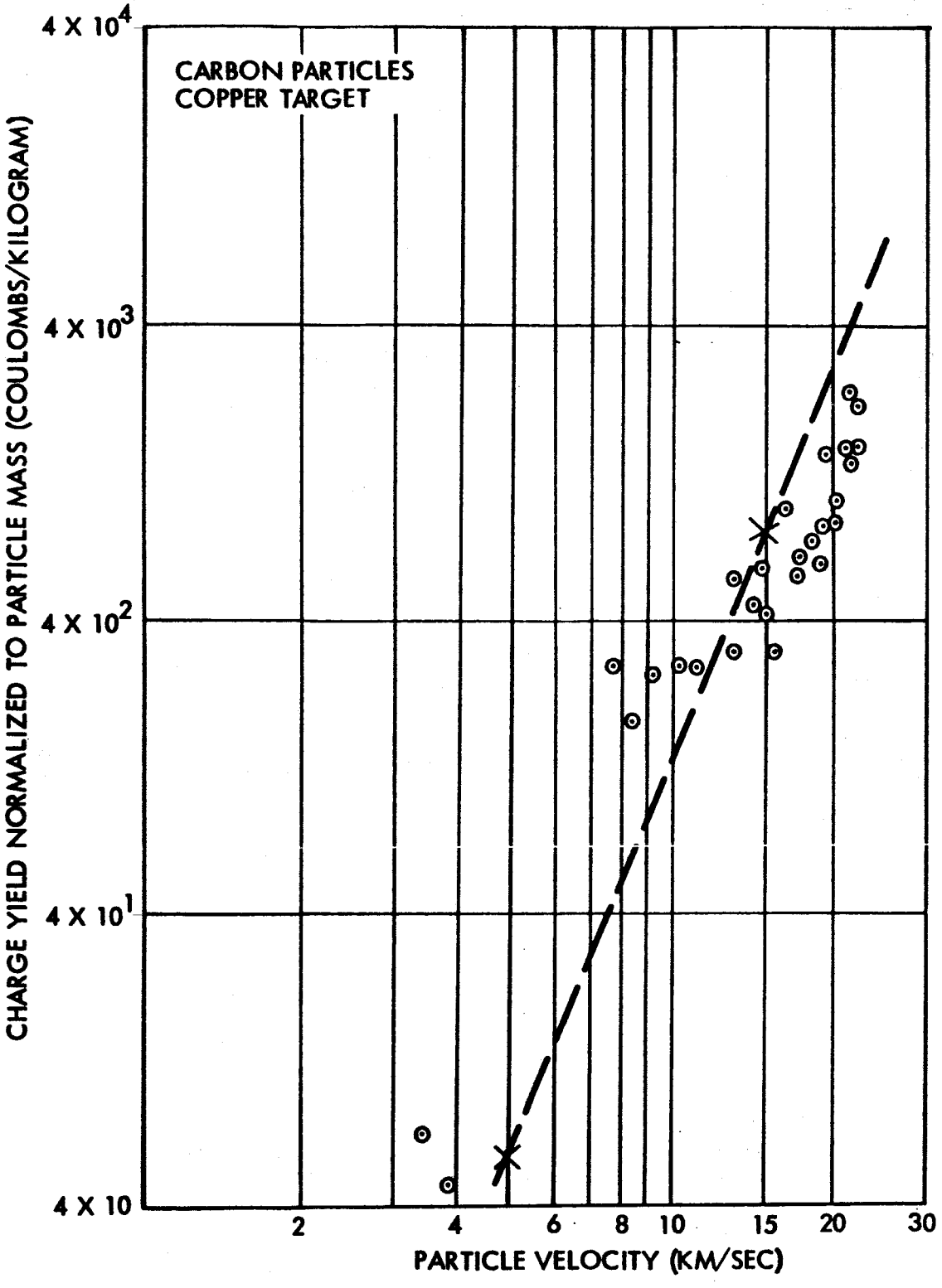

Figure 3. Charge Yield, Normalized to Particle Mass, from Carbon Particles Impacting on a Copper Target as a Function of Particle Velocity. Dotted line is an approximate fit to previous data using iron particles on the same target material.

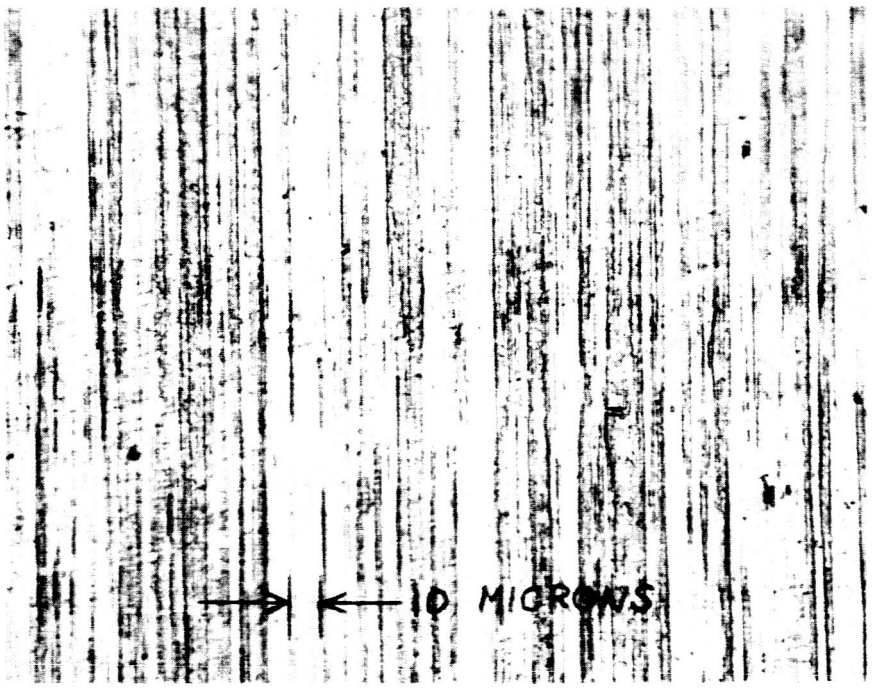

Figure 4a

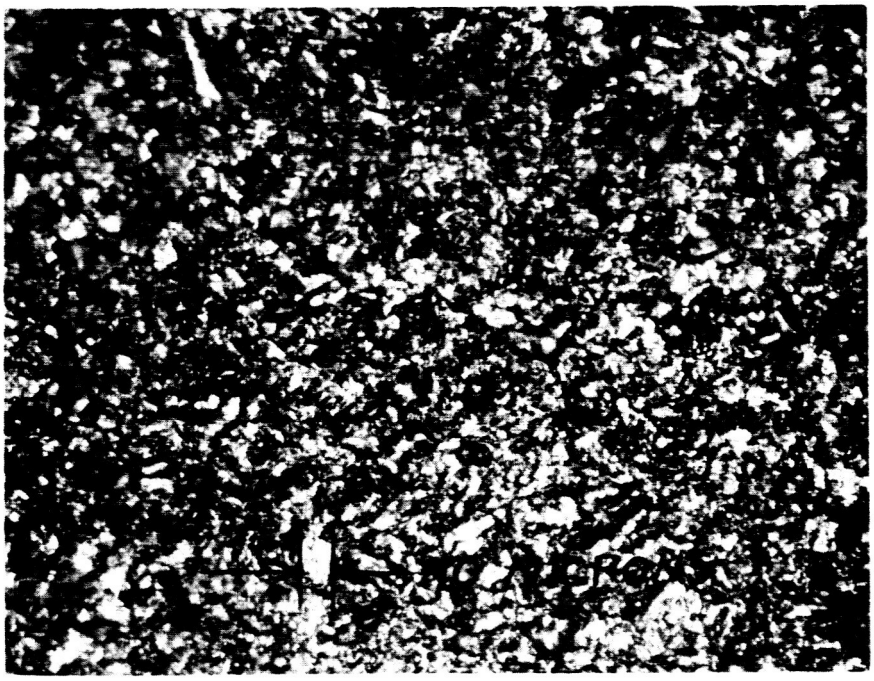

Figure 4b

Figure 4c

Figure 4. Microscope photographs of molybdenum target surfaces.

voltage went negative as a result. These data are shown in Fig. 5, where the charge yield, normalized to particle mass, is plotted against particle velocity for all three targets. In each case the charge on the incoming particle has been subtracted from the total charge.

There is some spread to the data, as usual in experiments of this kind. However, the points from the three different targets appear to be randomly distributed. At least there is no extreme departure from the curve for any particular target. It is worth mentioning that this set of data is a complete set in that no experimental points have been rejected for any reason. In Figs. 2, 3 and 5 each point plotted corresponds to a single particle collision.

If the local field were an important factor then one would expect to see at least some points which differed radically from the mean. For example, when a particle impacted on the bottom of one of the large craters, the local field must have been essentially zero. Since there appears to be no more spread than usual, the conclusion drawn is that the electric field at the target surface does not influence the amount of charge produced by an impact.

C. TIME-OF-FLIGHT EXPERIMENTS

A number of time-of-flight experiments were conducted on the positive and negative charge carriers produced in an impact. The experiments consisted simply of accelerating the charge through a known potential and then allowing it to drift through a field-free region to a collector. The charge-to-mass ratio was calculated from the transit time and the accelerating voltage.

The transit time of the negative charge carriers was so short it could only be compatible with electrons as the charge carriers. However, the positive charge carriers turned out to be more difficult to identify. It was almost immediately obvious that the charges were ions of a mass number less than 100 (assuming singly ionized particles), but that they were being ejected from the impact site with a substantial initial velocity.

Several accel-decel experiments were conducted in an attempt to measure the ion initial velocity in terms of the retarding potential the ions could overcome. The results were not conclusive, at least partially due to the spread in initial energies. However, it was established that an initial velocity does exit and corresponds to an energy of the order of ten electron volts for particles having velocities in the range 10 km/sec and lower.

The results of some of the time-of-flight experiments are given below. The flight path was 10.5 cm and the accelerating voltage varied from 100 to 300 volts. When iron particles were

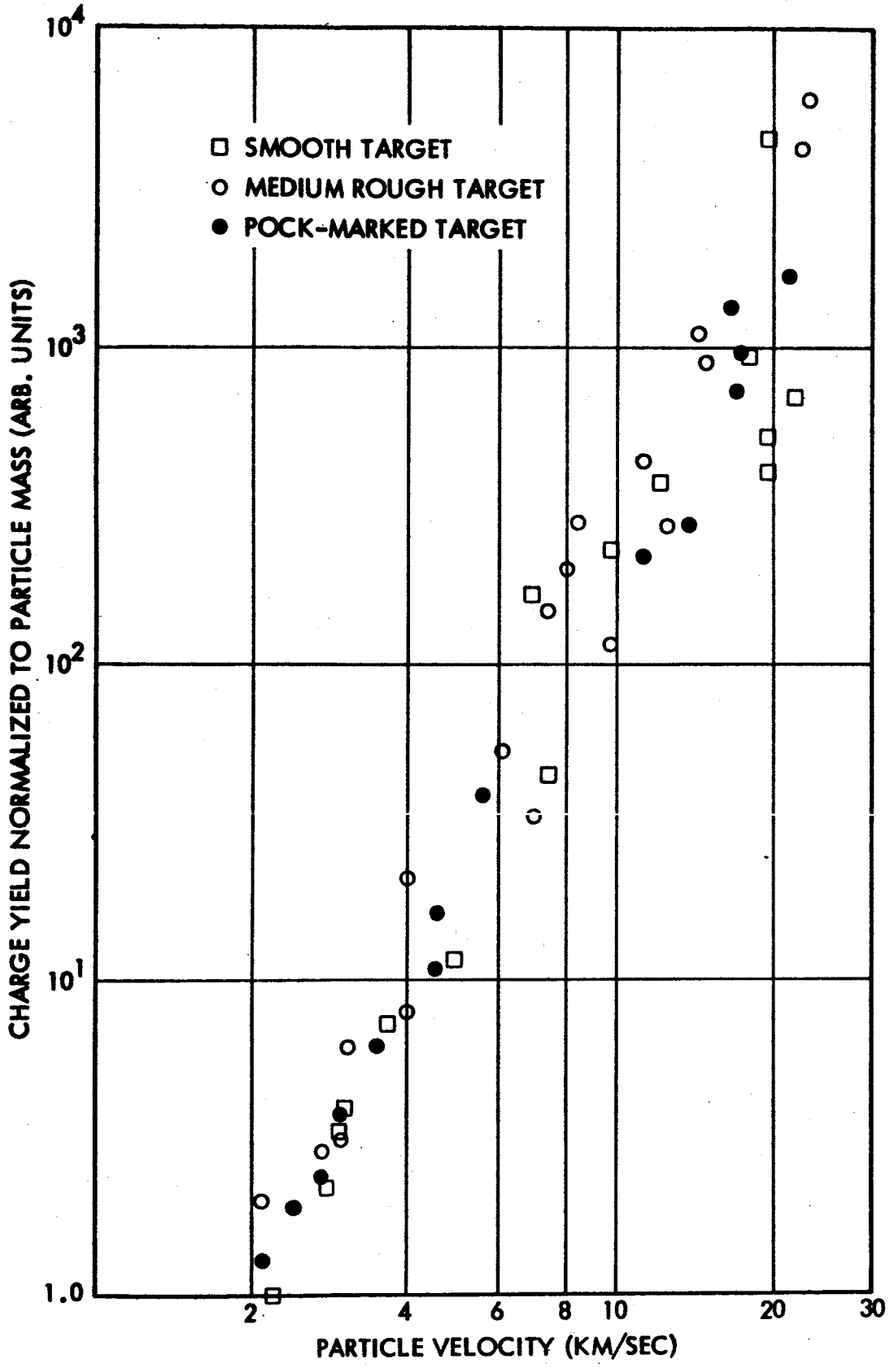

Figure 5. Charge emission due to impacting iron particles from molybdenum targets of different surface roughness.

used, two groups of ions appeared; the first group consisting of about 10% of the total charge and the second group consisting of about 90% of the total. In the case of carbon particles there were also two groups of ions; in this case the first group was about 33% of the total charge and the second group 66%. In Table I are listed the ion flight times over a 10.5 cm flight path, with different accelerating voltages, for ions from carbon and iron particle impacts. The results obtained did not depend on the target material, for the three materials used, tungsten, tantalum and molybdenum.

As in the case of iron particles, accel-decel experiments showed that ions from the carbon particle impacts could overcome at least 6 to 10 volts deceleration, indicating the existence of an initial velocity.

In Table II are listed the mass numbers calculated from the data in Table I, assuming singly ionized atoms and applying no initial velocity correction.

TABLE I - Measured Flight Times (μsecs)

Accelerating Voltage	Carbon Particles I(33%)	Carbon Particles II(66%)	Iron Particles I(10%)	Iron Particles II(90%)
100	3.25±0.04	4.33±0.04	4.08	5.22±0.14
200	2.31±0.03	3.04±0.04	3.00	3.81±0.15
300	1.84±0.05	2.46±0.04	2.43	3.14±0.04

TABLE II - CALCULATED MASS NUMBERS

Accelerating Voltage	Carbon Particles I(33%)	Carbon Particles II(66%)	Iron Particles I(10%)	Iron Particles II(90%)
100	18.5	32.8	29.0	47.3
200	18.7	32.4	31.2	50.5
300	18.2	31.8	30.8	51.4

Notice the similarity between Group II of the carbon particles and Group I of the iron particles. They are both close to mass 32, which could correspond to molecular oxygen. On the other hand, the mass number 18 of the first carbon group differs considerably from the expected value of 12, just as the mass number around 50 differs from the expected value of 56 in the case of iron. In the case of iron this difference might be explained by postulating an initial ion velocity, decreasing the flight time and lowering the calculated mass number. If this effect is present in the case of carbon particles, it would increase the calculated mass number of 18, instead of lowering it towards the expected value of 12. At the present time, no explanation exists for this apparent discrepancy, unless the ions are not carbon, but some chemical compound of carbon, possibly an oxide.

Considering the iron data alone, it is possible to apply a voltage correction to the measured accelerating voltages to make all the calculated mass numbers agree. (This correction would presumably correspond to the ion initial velocity.) Changing the accelerating voltage by 14 volts corrects the main ion group mass numbers to 53.9, 54.0 and 53.8. These numbers still differ by 4% from the expected value of 56. A 4% error in mass number is equivalent to a 2% error in time or distance measurement. The signals are such that the precision in time measurement is probably no better than $\pm$5%.

The net result of the time-of-flight experiments is not completely satisfactory. However, it is possible to make the following statements concerning the positive charge created by an iron particle impact in the 10 km/sec velocity range.

1. The charge carriers are emitted with an initial velocity which corresponds to an energy of the order of ten electron-volts.

2. 90% of the charge is carried by one group of ions and the spread in mass numbers of this group of ions is estimated to be less than $\pm$20%.

3. The mass number of this 90% group appears to be between 50 and 56 a.m.u.

Statements (2) and (3) rule out the possibility of any substantial amount of charge being carried by ions of target material (Mo has A = 96, Ta has A = 181, W has A = 184). This is true unless one postulates a mechanism which results in large numbers of doubly ionized ions and no singly ionized ions, which seems very unlikely. It is tempting to conclude that only the particle material is ionized and none of the target material.

Since there appeared to be a possibility that all the ions might be due to alkali metal impurities, a flame photometric analysis for sodium and potassium was performed on the iron and carbon particles used in the accelerator. The results were:

Carbon sample:	Na^+	= 0.048%
	K^+	= 0.004%
Iron sample:	Na^+	= 0.129%
	K^+	= 0.100%

It is felt that these impurities, particularly in the case of carbon, are too low to account for the observed ion emission.

D. ALUMINUM PARTICLES

At the start of the contract period, it was hoped that a sample of aluminum powder suitable for use in the accelerator could be obtained. This would have permitted comparison of data from three particle materials, aluminum, carbon and iron. The requirements on the powder used are that it be: 1) conducting, 2) spheroidal in shape with no sharp points, 3) that it have a size distribution which contains particles from about 0.1 micron diameter up to about 1 or 2 microns diameter and 4) that it contain very few particles larger than 5 or 10 microns.

A contractor was found who agreed to supply a suitable sample of aluminum powder. However, examination of the sample showed it to be completely unsatisfactory. The particles were jagged and averaged about 10 microns diameter. A search was made for other suppliers, but none could be located.

There was available in the laboratory a one-pound sample of aluminum microspheres manufactured by the Linde Company. This powder fulfilled all our requirements except that the majority of the powder was very large diameter. Several attempts were made to separate the smaller particles from the larger and finally an air flotation technique was devised. The results were not completely satisfactory but it was felt that they were good enough to warrant ordering more microspheres from Linde, even though the cost was $50 per pound. The yield of the separation process was very low and the one-pound sample had been almost completely consumed in developing the process.

Unfortunately, Linde is no longer manufacturing aluminum microspheres. They stated that the demand for the powder was too low to justify the use of their machine which was needed for other applications. They did not know of any other supplier of spherical aluminum powder in this size range.

At this point the search was abandoned and no further attempt was made to accelerate aluminum particles.

IV. EXPERIMENTS ON PARTICLE INDUCED DISCHARGES

A. DISCHARGE PROBABILITY

The relative probability of a particle causing a discharge was measured for a simulated ion engine, both with cesium present and without cesium. These data were examined for any dependence of discharge probability on particle parameters. The experiments consisted of a tantalum target facing a tungsten grid, with a 2.5 mm spacing. The grid was 100 mesh, made with 0.001 tungsten wire. Particles were injected through the grid and impacted the target. The voltage was applied to the grid while the target was grounded. Discharges were detected by a loop of wire which magnetically coupled to the high current which flowed through the grid lead when an arc formed between grid and target.

The grid voltage in these experiments was positive with respect to the target. This was done because discharges do not occur when the impact point is the positive electrode at these relatively low voltages (3-9kV).

A particle detector was located approximately 10 cm in front of the high voltage grid, and as each particle passed through the detector it was recorded on the electronic x-y plotter. There was a delay of 100 μsec associated with the x-y plotter and if a discharge occurred during this time interval, then the particle was plotted as a short line. If no discharge occured in the 100 μsec, the particle was plotted as a point. This display was photographed and particle parameters, velocity and radius, were read from it later. Only about fifty points or lines representing particles were usually put on one photograph.

Figure 6 shows the results of the experiments done with a clean system, with no cesium present. The percentage of particles causing a discharge is plotted against the high voltage applied between target and grid. Three sets of points are shown. They represent percentages calculated using all particles, particles with radii between 0.35 μ and 0.5 μ, and particles larger than 0.75 μ radius. At each setting of the high voltage, approximately 100 particles were recorded.

In Fig. 7 are plotted the results of a similar experiment with cesium sprayed onto the target and grid. The cesium gun was located about 1-1/4" below the target and grid. Cesium was evaporated until a film of cesium was observed to form on the transparent chamber covering about 3/4" above the target and grid. The three sets of points in Fig. 7 represent percentages calculated with the same particle parameters as those in Fig. 6.

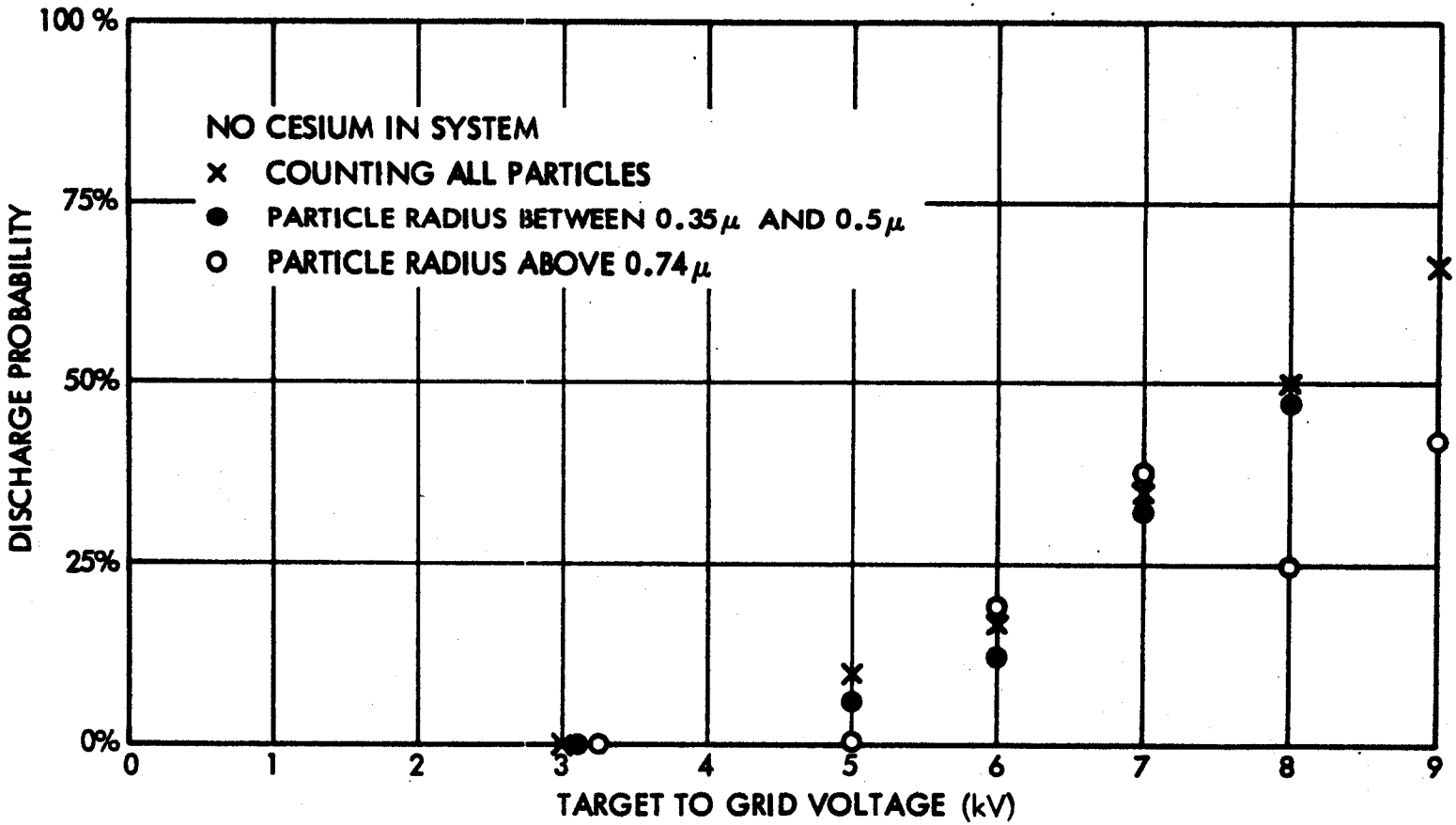

Figure 6. Probability of a particle impact initiating a discharge in a simulated ion engine as a function of ion engine grid voltage.

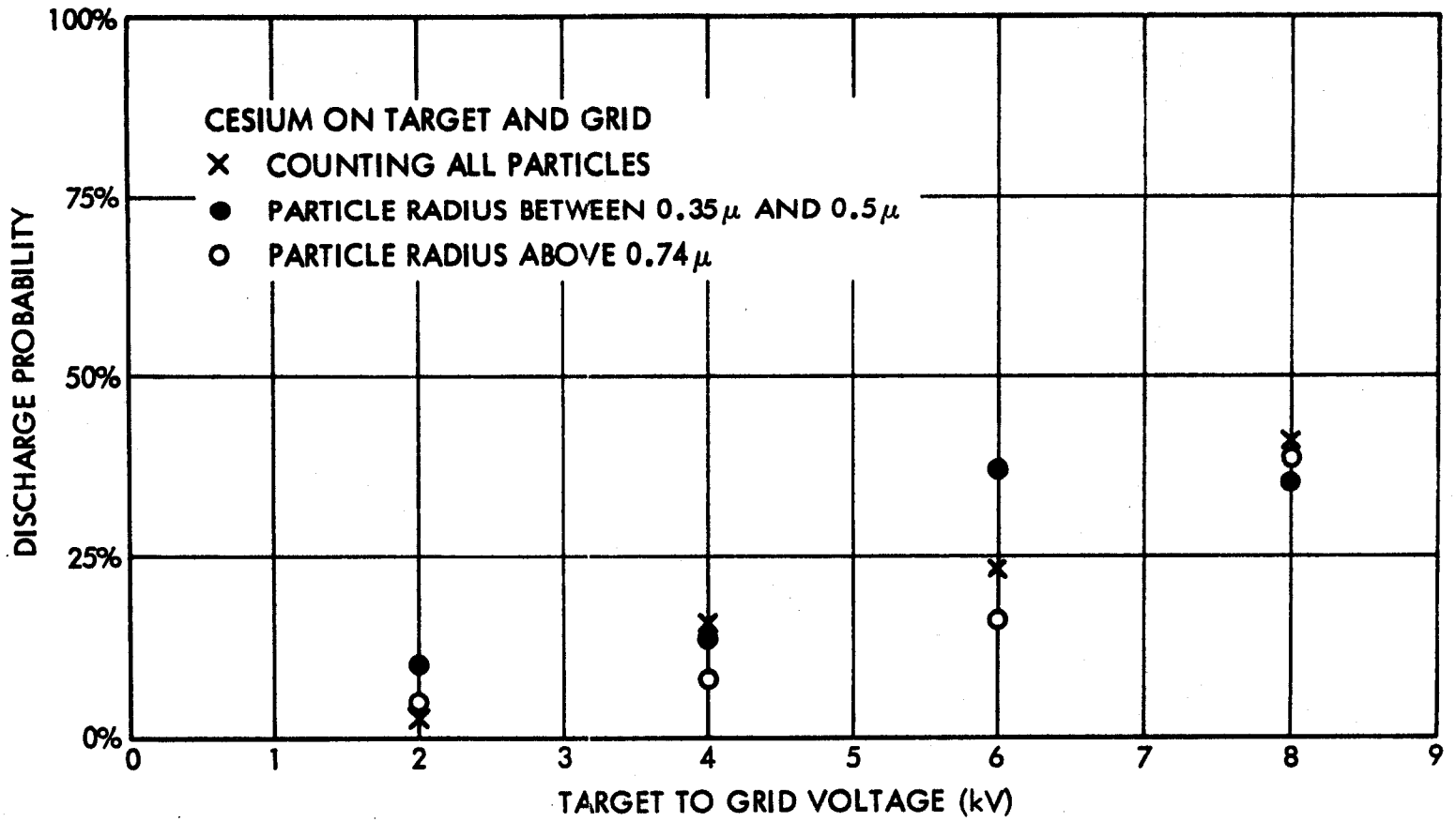

Figure 7. Probability of a particle impact initiating a discharge in a simulated ion engine as a function of ion engine grid voltage in the presence of cesium.

It may be seen from Figs. 6 and 7 that the probability of discharge increases with the applied voltage from a small number to as high as 50% at 8 or 9 kilovolts. The effect of particle size seems not to be significant. Within the scatter of the results, small particles have the same effect as larger ones; however, the spread in particle size is only a factor of about 4. The presence of cesium is noticeable at lower voltages where the probabilities with cesium present are somewhat higher. Above about 6 kV the cesium seems to make little difference. Actually, the probabilities with cesium in the system appear to be a little lower than the no-cesium ones at 8 kV, but not significantly.

The conclusions reached are that a particle from this accelerator has about a 50% chance of initiating a discharge in a system of this kind, with a moderately high voltage applied. This 50% probability drops considerably if the impact point voltage is positive with respect to its surroundings. In an ion engine, various voltages are present and possible micrometeorite impact points exist which are negative and others which are positive.

To say that the particle size has no effect is obviously an approximation. If the particle size is extrapolated down to one atom, there will certainly be no discharge, but at the present time the value of this cut-off in radius is not known. It may well be that there is no sharp cut-off, and instead a gradual transition in probability from high to zero.

B. DISCHARGE DAMAGE

Numerous experiments aimed at assessing the damage done by a typical discharge were performed. Most of these experiments relied on photography for damage analysis, but one set of targets was examined carefully for weight changes under repeated arcing.

Three copper targets and three tungsten targets were weighed and photographed before the experiment. They were then placed in the accelerator and bombarded until one, ten, and one hundred discharges occurred on separate targets. The target under bombardment was positioned about 0.100" away from a 100-mesh tungsten grid (positive) through a filtering system which is illustrated in Fig. 8. This set of filters is equivalent to that used on tests of the Lewis-Kaufman engine. The total voltage between grid and target was 6,000 volts.

It was obvious from the visual appearance of the discharge that the large inductors were very effective in limiting the current. Although the energy stored in the capacitors was equal to that used previously, the spark was much dimmer.

There was no measurable change in the target weights, to within 0.1 mg, after bombardment even with 100 discharges. The copper targets each weighed approximately 22.0 mg and the tungsten

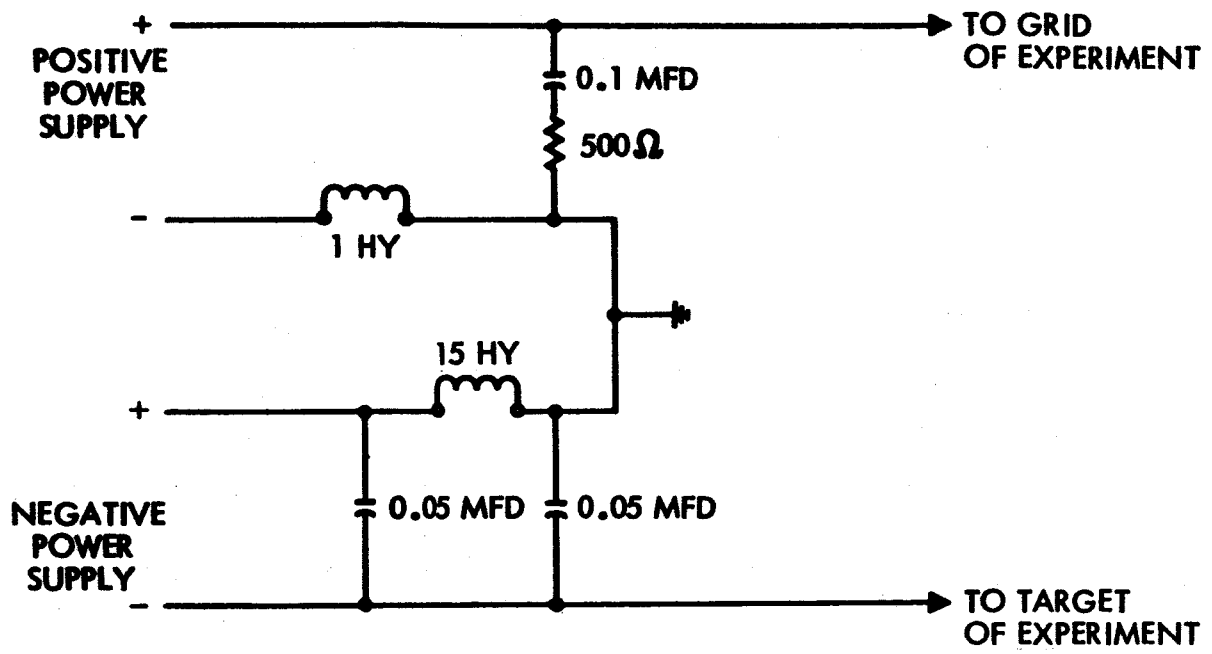

Figure 8. Filtering Circuit Used in Discharge Experiments.

targets 60.0 mg. One of the tungsten targets could not be weighed after the experiment because it was torn while being extracted. However, it was the target which has been exposed to only one discharge. The weights of the other five targets remained the same to within $\pm$0.1 mg.

This result is not very surprising when the extent of the damage, as shown in the photographs following, is examined.

Arc damage was examined microscopically for several target materials. In every case, the discharges were vacuum discharges caused by the impact of a hypervelocity particle and limited only by the external circuitry. The electrical filtering network is illustrated in Fig. 8. The filter circuit was supplied by Lewis Research Center.

The results obtained on tungsten targets are shown in Figs. 9 through 14. The tungsten target under bombardment was positioned about 0.100" away from a 100-mesh tungsten grid. Voltages were applied to the target (negative) and the grid (positive) through the filters shown in Fig. 8. Total voltage between target and grid was 6,000 volts.

Figures 9 through 11 show the same discharge site at three different magnificiations. The size scale is indicated in each photograph. This particular target was one which was impacted a large number of times, until about one hundred discharges had occurred. The discharge site shown in the photographs was selected at random and is fairly typical. There are actually two discharge sites visible in Fig. 9, outlined by circles. Only the central one is magnified further in Figs. 10 and 11. The small dots visible in all three photographs are craters created by the impacting particles. Particle craters are about 1 to 5 microns in diameter and usually quite circular.

The larger, irregularly-shaped craters are caused by the spark. The fact that one discharge will cause several small craters close to one another is a well-known characteristic of vacuum arcs. References 1 and 2, for example, both contain photographs of electrodes subjected to high-voltage vacuum breakdown which show crater formation similar to that illustrated here. These craters are actually smaller than the ones in Refs. 1 and 2, presumably because of the current limiting action of the external circuitry.

The appearance of Fig. 11 suggests that material from the crater sites may have been deposited in adjacent regions of the surface. All in all, the extent of the damage to the target surface is roughly equivalent to 20 or 30 particle impacts.

Figures 12, 13 and 14 are photographs of another discharge

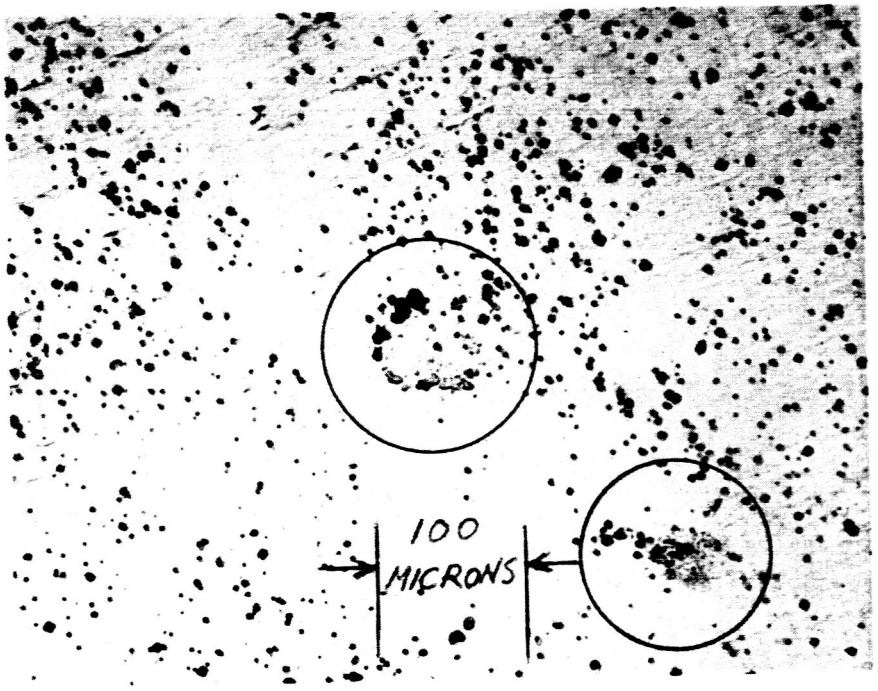

Figure 9. Site of Discharge Caused by Particle Impact on Tungsten Surface. Two discharge sites are visible, outlined by circles.

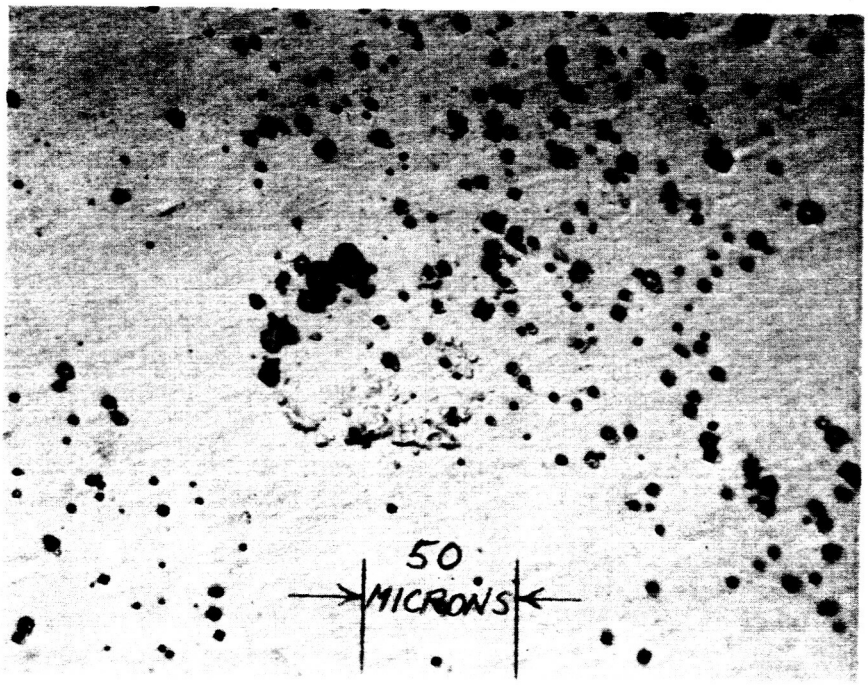

Figure 10. Further magnification of central discharge site shown in Fig. 9.

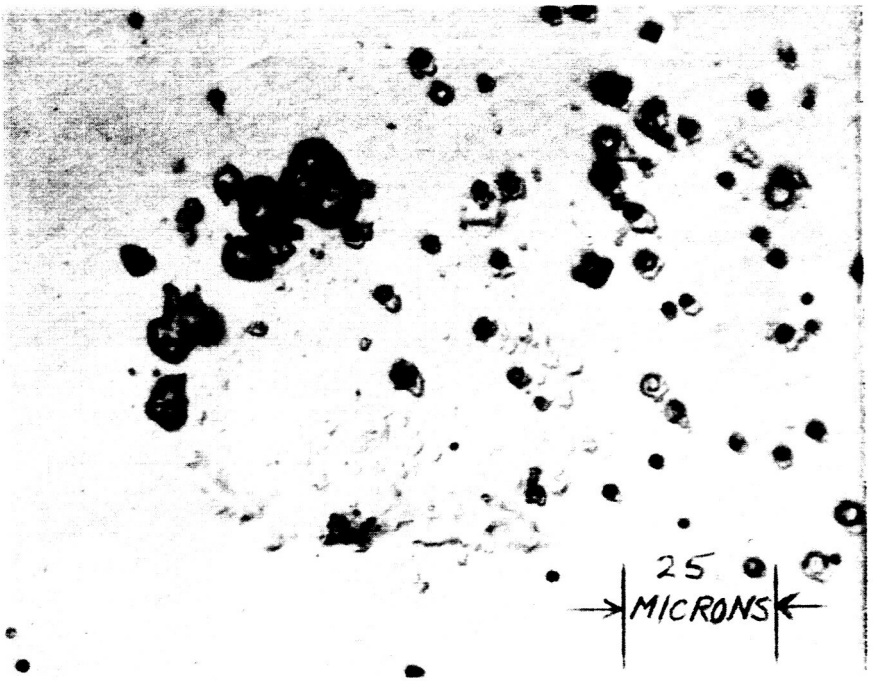

Figure 11. Central discharge site shown in Fig. 9. Small circular marks are particle craters. Large irregularly shaped areas are craters created by the discharge.

Figure 12 Discharge Site on a Tungsten Surface.

Figure 13. Further Magnification of Discharge Site Shown in Fig. 12.

Figure 14. Further Magnification of Discharge Site Shown in Fig. 13.

site on a tungsten target. This one occurred with only one impact and is in an area not surrounded by particle craters. It is included because it is somewhat atypical in that the multi-crater formation of the spark is not as apparent. This is not caused by the fact that the arc occurred in an area where there were few particle craters. Other spark sites have been observed which are in clear areas, but usually exhibit the structure shown in Fig. 11.

When this same type of experiment was conducted using copper electrodes, it was immediately obvious that the damage was considerably less. In fact, the experiments had to be repeated several times before any discharge sites could be located. It was only after the copper electrodes were subjected to painstaking polishing that it became possible to observe the site of an arc. Microscopic examination of the surface was also frustrating, and the final conclusion drawn was that any damage appeared only as a slight surface discoloration, with a slight enhancement of surface features such as a mild etching might produce.

Two photographs of a typical discharge site on a copper eletrode are shown in Figs. 15 and 16. The experimental arrangement was the same as that used for tungsten electrodes. The surface shown in Figs. 15 and 16 is very smooth and has a high reflectivity.

While performing a discharge experiment on one of the copper targets, the 500 ohm resistor in the filtering network was inadvertently left out of the circuit (see Fig. 8). This had the effect of permitting a 0.1 microfarad capacitor to discharge through the arc with no current limitation (other than the self-inductance and the lead inductance). The net result was that the amount of energy in each arc was greatly increased over that obtained with the high voltage filter correctly installed. This was apparent even from outside, as each spark was much brighter than expected.

There was no difficulty in locating these discharge sites on the copper surface, and microscope photographs of the surfaces are reproduced in Figs. 17, 18, and 19. These craters are considerably larger, consisting of a central depression about 0.001" in diameter and a raised circular lip. The lip is about 0.004" in diameter. Considering the difficulty experienced in locating discharge sites obtained with the correct high voltage filters, it is obvious that the filters are very effective.

A series of discharges were induced on aluminum electrodes and again the character of the damage differed considerably from either the tungsten or the copper, although the experimental conditions were identical. In this case, the damaged areas were very easy to locate even with only one discharge on a target. The affected area was very large (averaging about .020" diameter), and the surface appears to have melted and recrystalized in a granular

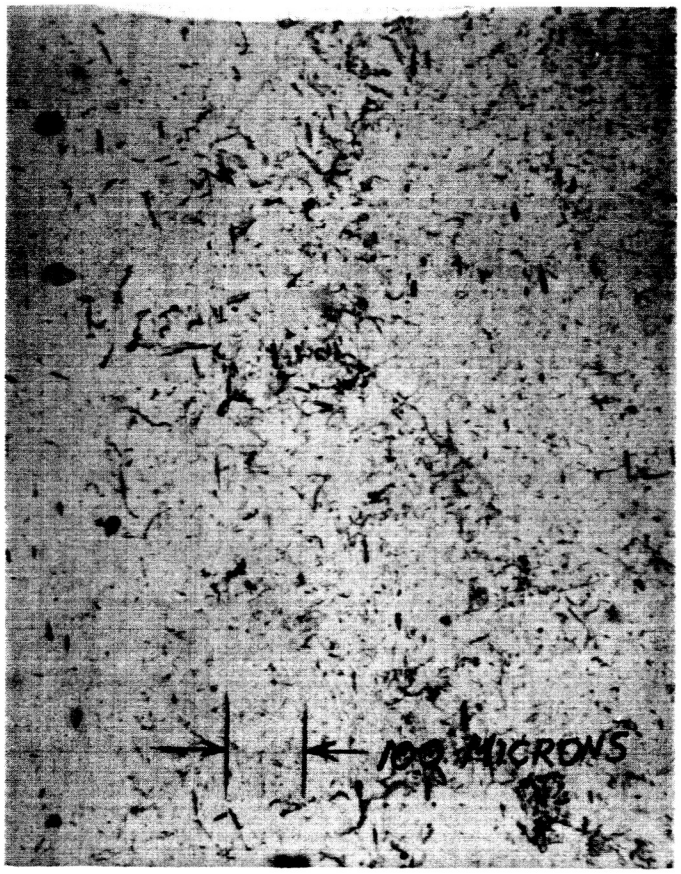

Figure 15. Discharge site on surface of copper electrode.

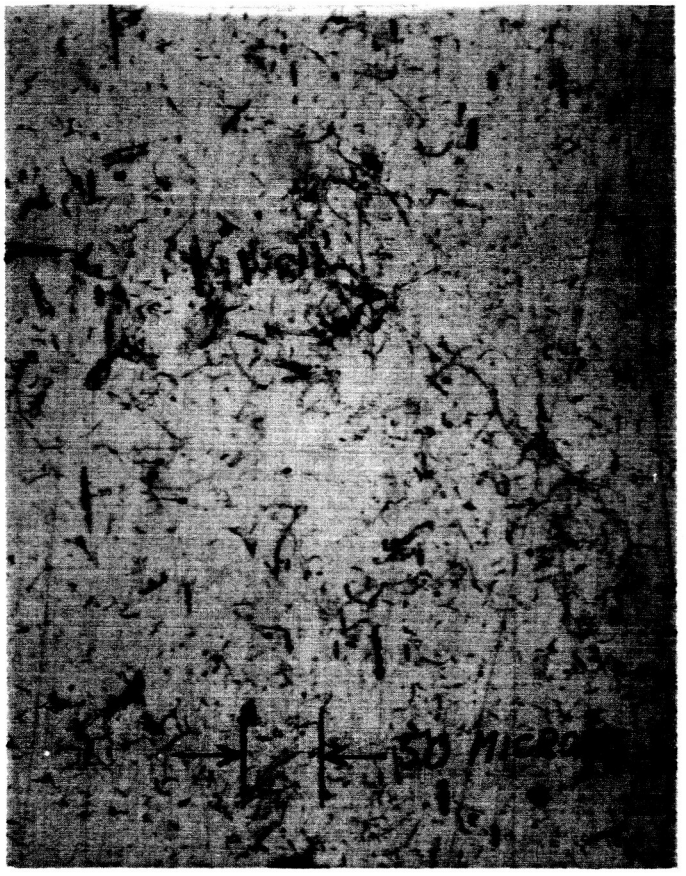

Figure 16. Further magnification of discharge rite shown in Fig. 15.

Figure 17. Discharge Sites from Particle Initiated Breakdown in Copper Target. Damage caused by energy stored in 0.1-μf capacitor.

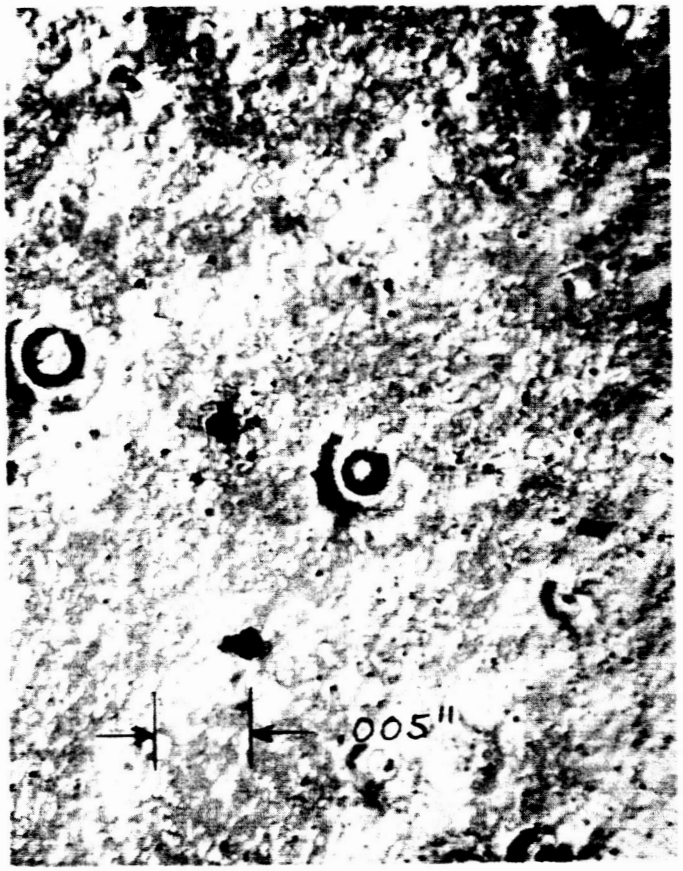

Figure 18. Further Magnification of Discharge Sites Shown in Fig. 17.

Figure 19. Further Magnification of Discharge Sites Shown in Fig. 18.

form. One of these discharge sites is shown in Figs. 20, 21, and 22. It would appear from the pictures that the damage does not penetrate into the metal as in the case of tungsten, but certainly the area covered is much greater.

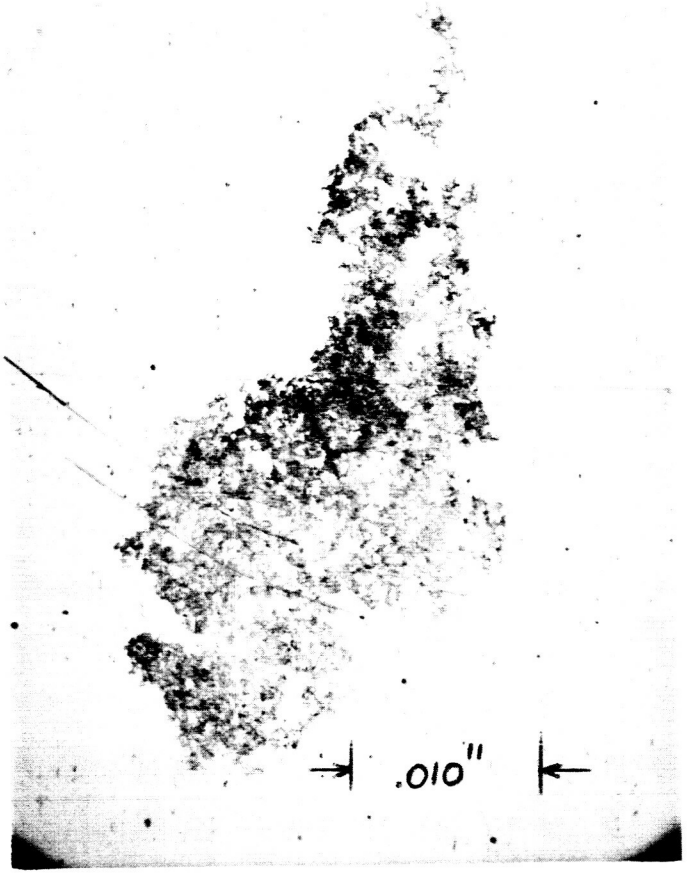

Figure 20. Discharge site on surface of an aluminum electrode.

Figure 21. Further magnification of discharge site shown in Fig. 20.

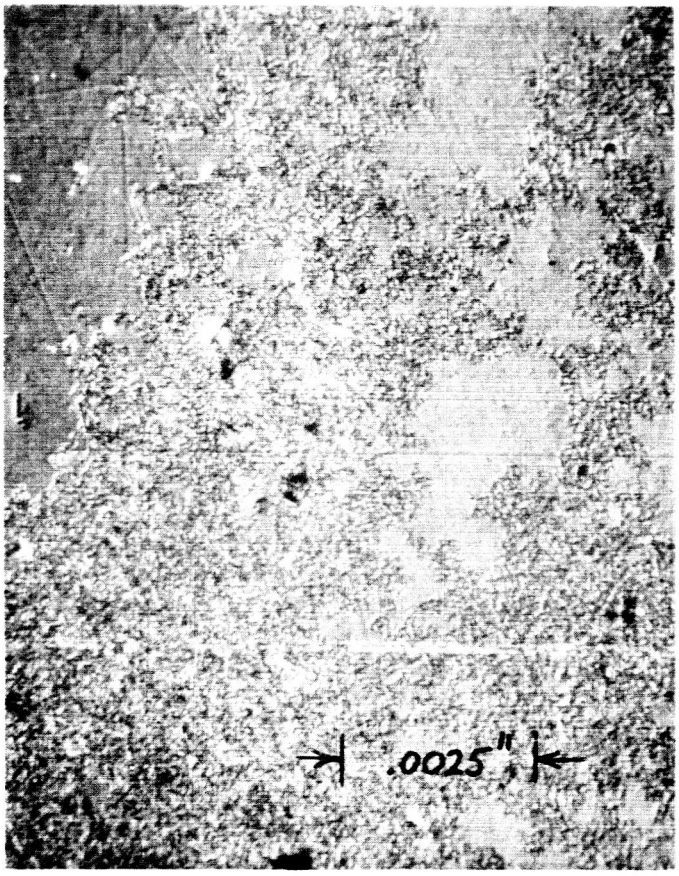

Figure 22. Further magnification of discharge site shown in Fig. 21.

V. CONCLUSIONS

The tentative model of particle-induced breakdown developed under the previous contract appears to be substantially correct. The impact of a small hypervelocity particle produces a cloud of gaseous vapor (along with some solid particles) which expands back from the impact point. There are also produced a number of ions and electrons, either by an unknown mechanism during the impact or by thermal ionization in the expanding gas. The ions appear to come from the particle material, with the target material contributing very little.

If there is enough material in this expanding gas cloud and the voltage and field are appropriate, there will be charge multiplication within the gas. This multiplication alone is not sufficient to produce an arc. However, if enough energy is delivered to the electrode by means of charge multiplication to start more material vaporizing, then the process becomes self-sustaining. It will continue to grow as long as energy is supplied externally. The probability of a particle initiating this breakdown can be as high as 50%, with moderate voltages.

The purpose of any external electric filtering network is to limit the amount of energy available. This is done by placing resistors and inductors in series such that any sudden current surge is accompanied by a large voltage drop. When the voltage across the gap is decreased sufficiently the arc is extinguished. Judging from the damage pictures contained in this report, the filtering circuit used (which was supplied by Lewis personnel) accomplishes its purpose very well.

The actual damage caused to electrodes with the filter in place is not really very large. On tungsten electrodes the net effect was equivalent to about 20 or 30 small particle impacts. On the other hand, any damage to copper electrodes was virtually zero. The effect on the aluminum electrodes was to give a relatively large surface area a "frosted" appearance. In a large number of applications neither the surface pitting nor the surface "frosting" will interfere with the electrode function.

REFERENCES

1. A. S. Denholm, Can. J. of Phys., 36, 476 (1958).

2. A. Maitland, J. Appl. Phys., 32, 2399 (1961).

DISTRIBUTION LIST FOR SUMMARY REPORT

CONTRACT NAS 3-5755

Addressees	Copies
NASA-Lewis Research Center Spacecraft Technology Procurement Section 21000 Brookpark Road Cleveland, Ohio 44135 Attention: John H. DeFord	1
NASA-Lewis Research Center Electromagnetic Propulsion Division 21000 Brookpark Road Cleveland, Ohio 44135 Attention: H. R. Kaufman	1
P. D. Reader	1
W. E. Moeckel	1
E. A. Richley	
NASA-Lewis Research Center Spacecraft Technology Division 21000 Brookpark Road Cleveland, Ohio 44135 Attention: D. L. Lockwood	1
J. H. Childs	2
J. A. Wolters	1
R. R. Nicholls	1
John Ferrante	5
NASA-Lewis Research Center Technology Utilization Office 21000 Brookpark Road Cleveland, Ohio 44135 Attention: John Weber	1
NASA-Lewis Research Center Technical Information Division 21000 Brookpark Road Cleveland, Ohio 44135	1
NASA Headquarters FOB-10B 600 Independence Avenue, S.W. Washington, D. C. 20546 Attention: RNT/James Lazar	2
Dr. Maurice Dubin	1
NASA Marshall Space Flight Center Huntsville, Alabama 35812 Attention: M-RP-DIR/Dr. E. Stuhlinger	1

Addressees	Copies
NASA Langley Research Center Langley Field, Virginia Attention: Technical Library	1
Headquarters - USAF Air Force Office of Scientific Research Washington, D. C. 20525 Attention: Dr. M. Slawsky	1
Commander Aeronautical Systems Division Wright-Patterson Air Force Base, Ohio 45433 Attention: AFAPL (APIE)/Robert Supp	1
NASA-Lewis Research Center 21000 Brookpark Road Cleveland, Ohio 44135 Attention: Library	2
NASA-Lewis Research Center 21000 Brookpark Road Cleveland, Ohio 44135 Attention: Reports Control Office	1
AFWL Kirtland AFB, New Mexico Attention: WLPC/Capt. C. F. Ellis	1
Jet Propulsion Laboratory Pasadena, California Attention: J. J. Paulson	1
Aerospace Corporation P. O. Box 95085 Los Angeles, California 90045 Attention: Library Technical Documents Group	1
North American Aviation, Inc. 12214 Lakewood Avenue Downey, California Attention: Technical Information Center Dept. 4096-314	1
Colorado State University Fort Collins, Colorado Attention: L. Baldwin	1

Addressees	Copies
Hughes Research Laboratories 3011 Malibu Canyon Road Malibu, California 90265 Attention: Dr. G. R. Brewer	1
Mr. R. C. Knechtli	1
Field Emission Corporation 611 Third Street McMinnville, Oregon Attention: Dr. F. M. Charbonnier	1
United Aircraft Corporation Research Department East Hartford, Connecticut Attention: Dr. R. G. Mayerand, Jr.	1
Westinghouse Astronuclear Laboratories Pittsburgh, Pennsylvania 15234 Attention: H. W. Szymanowski, Manager Electrical Propulsion Laboratory	1
Aerojet General San Ramon, California Attention: Dr. J. S. Luce	1
Electro-Optical Systems, Inc. 125 North Vinedo Avenue Pasadena, California Attention: Dr. A. T. Forrestor	1
U. S. Atomic Energy Commission Division of Technical Information Extension P. O. Box 62 Oak Ridge, Tennessee 37831	1
NASA Scientific and Technical Information Facility Box 5700 Bethesda, Maryland Attention: NASA Rep. RQT 2448	6
Information Processing Section Wright-Patterson AFB, Ohio Attention: ASRCEM	1
Department of Physics Hiram College Hiram, Ohio Attention: Prof. Laurence Shaffer	1